



Novel approach to prepare carbon-encapsulated CIPs@FeO composite for efficient absorption of low-frequency microwave

Pengfei Yin¹ · Limin Zhang² · Ping Sun³ · Wenjuan Wu¹ · Xiyuan Sun¹ · Xing Feng¹ · Jian Wang¹ · Jianwu Dai⁴ · Yuting Tang¹

Received: 19 February 2020 / Accepted: 20 May 2020 / Published online: 27 May 2020
© Springer Science+Business Media, LLC, part of Springer Nature 2020

Abstract

Due to the urgently demand of microwave absorption materials in the low-frequency band, herein the CIPs@FeO@C multi-layer core-shell composite with advisable low-frequency microwave absorption performance has been successfully synthesized by a novel co-calcine, high temperature thermal diffusion and reduction method. The excellent attenuation characteristic, good impedance matching property, efficient eddy current loss, Debye relaxation and interfacial polarization etc. contribute to this desirable low-frequency electromagnetic absorption performance. The broadest effective absorption bandwidth in low-frequency range is 1.2 GHz and the maximum RL is -24.64 dB at 1.88 GHz for 4 mm and 6 mm, respectively. The as-prepared ternary composite has a great potential in production of low-frequency microwave absorption materials for the delightful performance and economical preparation method.

1 Introduction

Nowadays, owing to the fast evolution of electrommunication technique and precision electromagnetic equipment, the radiation of superfluous electromagnetic-wave leading to the electromagnetic pollution have become a growing problem, which is harmful to the human health and form the electromagnetic interference (EMI) as well [1–4]. Thus, a great deal of microwave absorbing materials (MAMs) with high efficiency performance have been investigated, such as ferrites [5, 6], carbon-based materials [7–9], conducting polymers [10, 11], magnetic metals [12, 13], dielectric ceramics [14, 15] and so on. Among these MAMs, the carbonyl iron

powders (CIPs) have been broadly applied in electromagnetic absorption field due to its high saturation magnetization and low cost [16]. However, the electromagnetic absorbing performance of pure CIPs is very limited, especially in the low-frequency band, owing to the toneless electromagnetic absorption mechanism, poor impedance matching condition etc., hence, various improved strategy to optimize the electromagnetic absorbing properties of CIPs have been proposed by many scholars. For instance, Zuo et al. [17] used digital light-processing three-dimensional printing technology to prepare graphene/CIPs/PMMA nanocomposites with decent electromagnetic-wave absorption performance, the maximal reflection loss (abbreviated as RL) of -54.4 dB for 2.1 mm thickness with an effective absorbing bandwidth of 3.41 GHz can be reached; Dong et al. [18] investigated the different geometries of CIPs on the final electromagnetic-wave absorption properties of CIPs/polyimide composite, which revealed that the electromagnetic-wave absorbing peak of flake-like CIPs is far lower than that of spherical CIPs for about 5.2 GHz, and the maximal RL peak value of -19.28 dB appeared at 11.62 GHz for a thickness of 1.5 mm; X. Chai et al. [19] used flake CIPs and chopped carbon fibers as raw materials to manufacture the thin electromagnetic-wave absorption patches via a simple tape-casting technology, the oriented FCI/CF/PMER patches exhibit commendable flexibility and showed a wide absorption bandwidth of 11 GHz with $RL < -5$ dB; Analogously,

✉ Pengfei Yin
yinpengfei@sicau.edu.cn

¹ College of Science, Sichuan Agricultural University, Ya'an 625014, People's Republic of China

² School of Science, Northwestern Polytechnical University, Xi'an 710072, People's Republic of China

³ Information Materials and Device Applications Key Laboratory of Sichuan Provincial Universities, Chengdu University of Information Technology, Chengdu 610225, People's Republic of China

⁴ College of Mechanical and Electrical Engineering, Sichuan Agricultural University, Ya'an 625014, People's Republic of China

Nan et al. [20] prepared oriented Fe microfiber and flake-like CIPs/epoxy hybrids by using a tape-casting equipment as well, an effective absorption frequency range of 3.5–18 GHz with reflection loss $RL < -8$ dB was achieved with the thicknesses from 1 to 2 mm; Moreover, Dai et al. [21] synthesized yolk-shell structured CIPs@void@nitrogen-doped carbon nanocomposite via the alkaline hydrothermal etching method, the maximal RL reached -25.7 dB at 17.2 GHz with an effective absorption bandwidth of 11.1–18 GHz, indicating that the preparation of core-shell structured CIPs composites is an effectual strategy to improve the electromagnetic property of CIPs indeed.

However, the low-frequency microwave absorbing properties of these CIPs-based composites is still very limited, and it requires a great improvement for that the outstanding low-frequency microwave absorption performance is urgently demanded at present stage. Such as the superfluous microwave radiation generated from electrical device in daily-life is mainly focus in the low-frequency range, which is very harmful to our human health and may cause the proliferation of cancer cell in the human body. Moreover, the detective frequency range of many ship-borne and phased-array radars has been gradually expanded to the low-frequency range as well. As a consequence, how to improve the electromagnetic absorption performance of CIPs-based composites in this range is worthy to be excavated.

Herein, we prepared a core-shell-shell structured CIPs@FeO@C nanocomposite via a novel co-calcine, high temperature thermal diffusion and reduction method with activated carbon as carbon source and reducing agent. The microwave absorption property of this multilayer core-shell composite, especially the absorption ability in low-frequency range has been rarely reported. In this work, the XRD, SEM, TEM and VNA were used to characterized the phase structures, micromorphology and microstructures, distribution of component elements, electromagnetism parameters, electromagnetic-wave absorption capacity of this MAMs, moreover, the

corresponding electromagnetic absorbing mechanisms have been also discussed. The results showed that the as-prepared CIPs@FeO@C composite can be applied as an effective low-frequency absorber for its superior performance and economical processing method.

2 Experimental methods

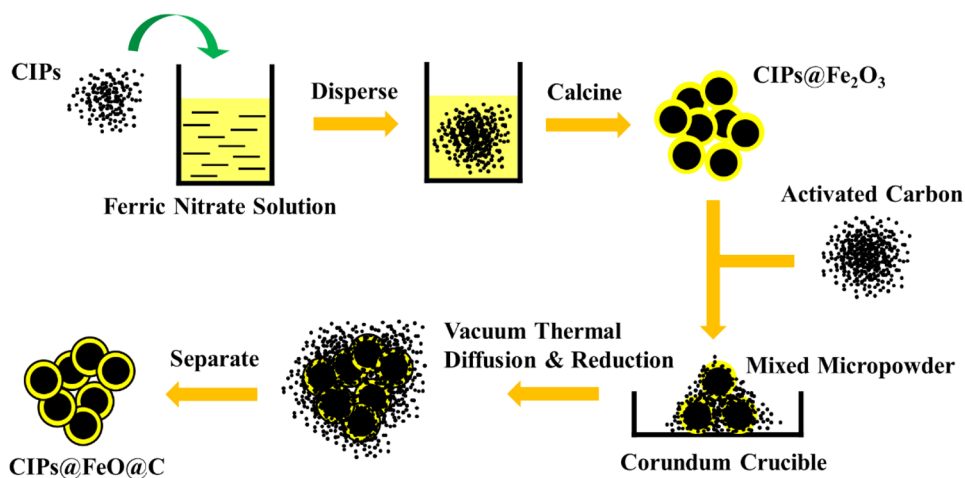
2.1 Materials

The CIPs micropowder was purchased from Lijia Metal Materials Co. Ltd., China. The iron nitrate nonahydrate ($\text{Fe}(\text{NO}_3)_3 \cdot 9\text{H}_2\text{O}$) was purchased from Keshun Biotechnology Co. Ltd., China. The activated carbon micropowder was obtained from Yatai United Chemical Co. Ltd., China. The purity of raw materials which were used as received are all higher than 99% percent.

2.2 Preparation of CIPs@Fe₂O₃ and CIPs@FeO@C composites

Figure 1 displays the preparation process of target composite in detail, the micropowder of raw CIPs was pre-washed with deionized water and dried for later use. First, 8.08 g iron nitrate nonahydrate was dissolved in 20 mL distilled water to form a diaphanous yellow solution, after that 20 g washed CIPs was subsequently added in the above solution and maintain the homogeneous mixing for 20 mins, then the turbid liquid was poured into an open container and hold the temperature at 300 °C for 20 h in an electric muffle, thus the obtain reddish-brown powder was CIPs@Fe₂O₃ composite. Afterwards, 7 g as-prepared CIPs@Fe₂O₃ composite was well-mixed with 14 g activated carbon to form the uniform powder, which was later put in a corundum crucible and calcined to 600 °C for 3 h in the vacuum tube furnace with a heating rate of 5 °C/min. After cooling down to the indoor

Fig. 1 Detailed preparation process schematic diagram of CIPs@FeO@C



temperature, the product was washed up with distilled water and screened out of mixed liquid by magnet for many times to remove the remaining impurities, then the final black powder of core–shell–shell structured CIPs@FeO@C composite was dried at 50 °C for 6 h.

2.3 Characterization

The crystal phase structure of as-prepared composites was characterized by X-ray diffractometer of D8-ADVANCE by using Cu- K_{α} radiation at a scan step of 0.02°. The morphology and structure of composites were observed by scanning electron microscope of SU8010. The high-resolution transmission morphology, elements distribution and selected area electron diffraction (SAED) of CIPs@FeO@C composite were tested by transmission electron microscopy of Tecnai G2 F30. Finally, the composites for measurement of electromagnetic parameters were homogeneously mixed with paraffin in 50 wt%, and the hybrids were compressed into a cylindrical shape with 2 mm thickness, $\Phi_{\text{out}} = 7.00$ mm and $\Phi_{\text{in}} = 3.04$ mm. Then, the S parameters of samples could be measured via vector network analyzer of TIANDA TD3618C within 0.5–3 GHz by using the coaxial transmission and reflection method, thus the electromagnetic parameters of relative permittivity and permeability can be calculated on the basis of NRW's theory [22, 23]. Therewith, the electromagnetic-wave absorbing properties of MAMs can be represented via the parameter of reflection loss rate (denoted as RL henceforth), which could be deduced by transmission-line theory based on the measurement of electromagnetic parameters as follows [24–26]:

$$Z_{\text{in}} = Z_0 \sqrt{\frac{\mu_r}{\epsilon_r}} \tanh \left(j \frac{2\pi f d}{c} \sqrt{\mu_r \epsilon_r} \right) \quad (1)$$

$$RL = 20 \log \left| \frac{Z_{\text{in}}/Z_0 - 1}{Z_{\text{in}}/Z_0 + 1} \right| \quad (2)$$

where, f is the frequency of electromagnetic-wave, c is the speed of light, d is the thickness of sample, Z_{in} and Z_0 are the input impedance of absorber and the impedance of free space, μ_r and ϵ_r are the relative permeability and permittivity, respectively.

3 Results and discussion

3.1 Structure and morphology analysis

Figure 2 displays the XRD spectrum lines of raw CIPs, CIPs@Fe₂O₃ and CIPs@FeO@C composites, it indicates that there are three characteristic diffraction peaks at $2\theta = 44.63^\circ$, 65.26° and 82.72° , which are in good agreement

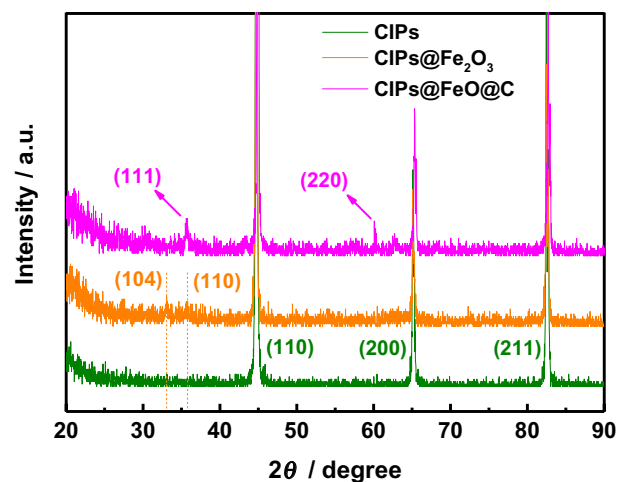


Fig. 2 X-ray diffraction patterns of raw CIPs, CIPs@Fe₂O₃ and CIPs@FeO@C composites

with the (110), (200) and (211) lattice planes of raw CIPs (JCPDS card No. 06-0696). With the cladding of Fe₂O₃ NPs on CIPs surface, as estimated, the weak characteristic diffraction peaks at $2\theta = 33.15^\circ$ and 35.61° are assigned to the (104) and (110) lattice planes of Fe₂O₃ (JCPDS card No. 33-0664), confirming the formation of Fe₂O₃ component composited with the CIPs; however, the intensity of these diffraction peaks are too weak compared with those of CIPs due to the thin thickness of cladding layer. It is interesting to note that the characteristic diffraction peaks at $2\theta = 35.48^\circ$ and 60.13° of CIPs@FeO@C composite are corresponding to the lattice planes of (111) and (220) in FeO (JCPDS card No. 06-0615), and there is nothing impurity peaks can be observed, suggesting that the Fe₂O₃ component was completely reduced by activated carbon under high temperature, moreover, the diffraction peak of encapsulated carbon layer generated from thermal diffusion process can not be measured for the thickness of which is too thin to be detected and the amorphous state.

Figure 3 presents the scanning electron photomicrograph of raw CIPs, CIPs@Fe₂O₃ and CIPs@FeO@C composites. As shown in Fig. 3a and b, the shape of raw CIPs displays irregular near-spherical with different sizes, and the surface of particle is relatively smooth as well. After the cladding of Fe₂O₃ component, it can be noted that the surface of CIPs presents a rough and porous state, which is made up by a large number of Fe₂O₃ NPs recognized from Fig. 3d. These loose porous structures and multi-interfaces may be beneficial to the electromagnetic absorption of incident microwave. Moreover, as shown in Fig. 3e and f, it suggests that the compactness of surface coating layer has been enhanced via the thermal diffusion and reduction treatment, attributing to the thermal migration process of cladding carbon from activated carbon to the surface of particles and the reduction

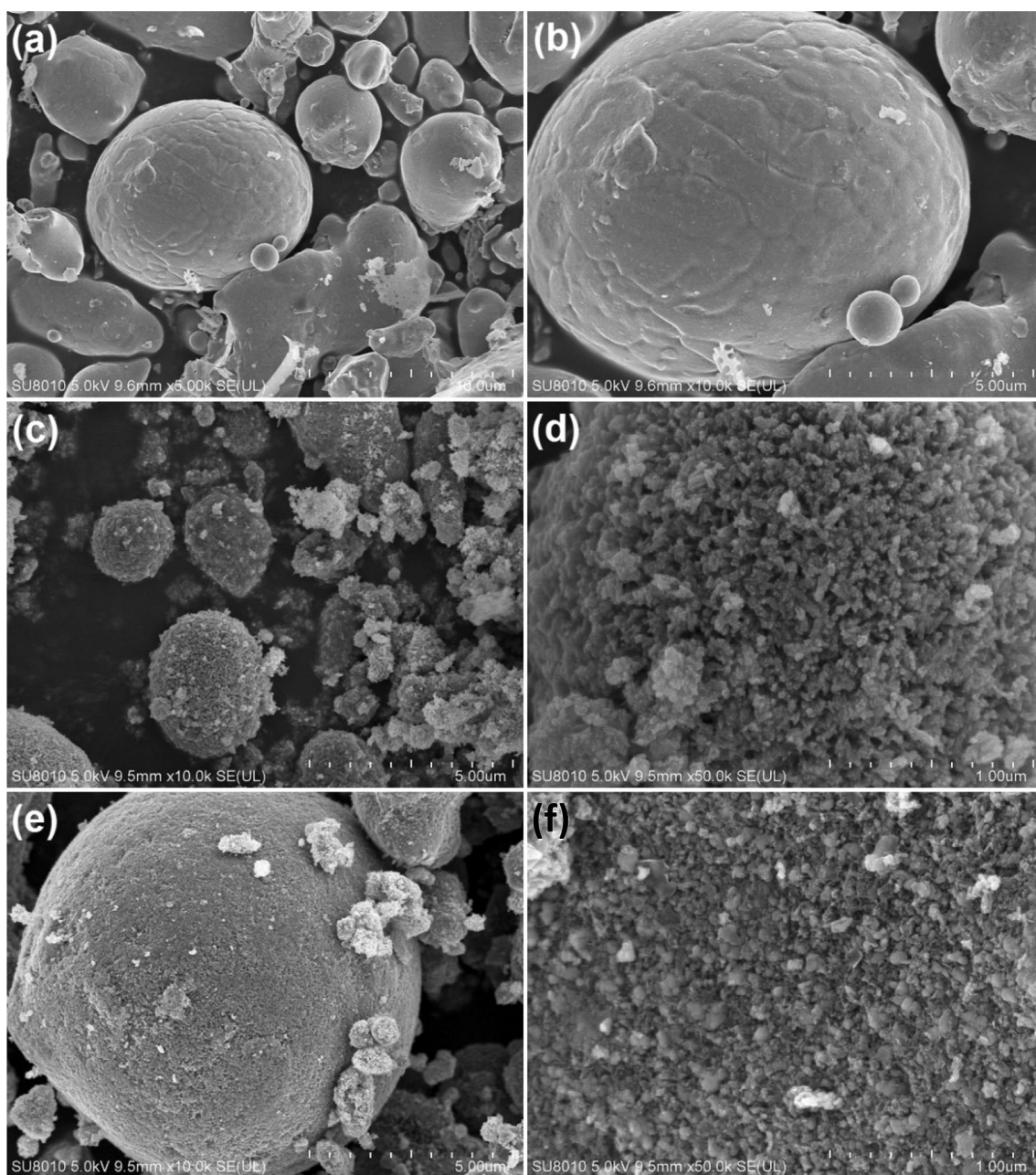


Fig. 3 Scanning electron photomicrograph with different magnifications of raw CIPs (a) and (b), CIPs@Fe₂O₃ (c) and (d), CIPs@FeO@C (e) and (f)

process of Fe₂O₃ NPs, hence, the surface impedance matching characteristics between particles and free space would be further improved with encapsulated carbon, which is also conducive to the incidence of microwave to be dissipated in the MAMs.

Transmission electron microscope images with low magnification, high-resolution TEM images and selected area electron diffraction (SAED) pattern of CIPs@FeO@C composite are expressed in Fig. 4. It is distinctly seen the encapsulated structure of particle in Fig. 4a and b, as well as

the shell is composed by a mass of nanocrystals. As shown in HR-TEM images of Fig. 4d and e, the distinct interplanar crystal spacing of 0.252 nm is corresponding to the (111) plane of FeO NPs, furthermore, it can be seen the encapsulated carbon layer of ~2 nm on the surface of FeO NPs as well. The selected area electron diffraction pattern in Fig. 4f shows many diffraction rings assigned to the (211), (200), (110) lattice planes of CIPs and (220), (111) lattice planes of FeO, respectively, suggesting the polycrystalline structures of composite. Meanwhile, Fig. 5 presents the EDS spectrum,

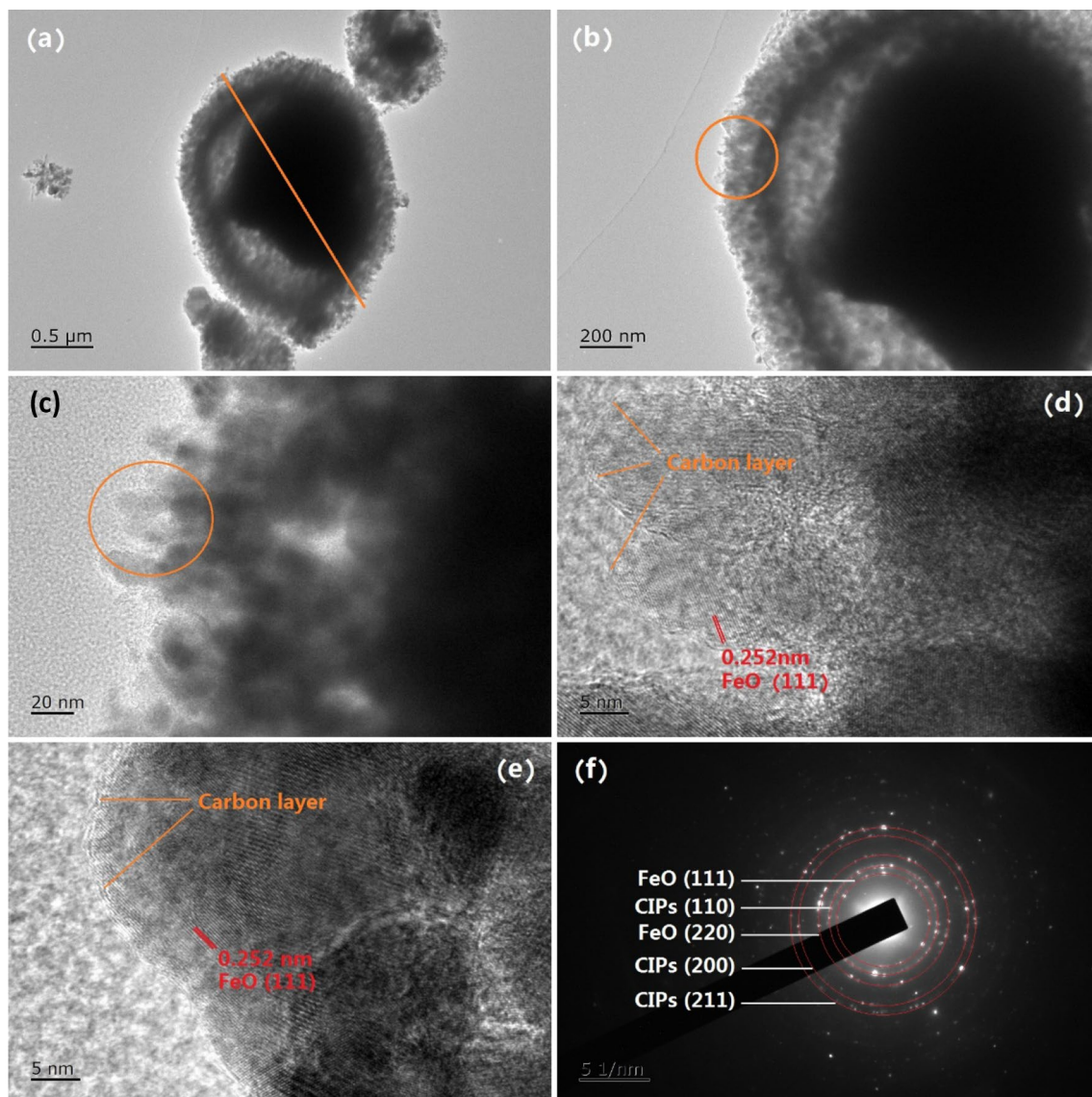


Fig. 4 Transmission electron microscope images of different magnifications (a) to (c), high-resolution TEM images (d) and (e), and SAED pattern (f) of CIPs@FeO@C composite

elements distribution on the surface of particle and along the characteristic line marked in Fig. 4a. It indicates that the Fe element is mainly concentrated in the core area on behalf of CIPs, and small amount of Fe element in shell is due to the cladding layer of FeO NPs; however, the O element is obviously concentrated in the area of shell part existing in FeO layer. Besides, it can be recognized in Fig. 5c that the distributed acreage of C element is slightly broader than that of O element, indicating the carbon-encapsulated configuration on the surface layer of as-prepared ternary composite. The EDS image in Fig. 5d also illustrates the composite only contains Fe, O, and C elements, further certifying the elementary composition in some extent. In addition, the distribution of Fe, O, C elements along the characteristic line

in Fig. 5e suggests that the shell of FeO surrounds the CIPs core, and then be encapsulated with a thin layer of carbon.

3.2 Microwave absorbing properties

Figure 6 shows the microwave reflection loss curves of raw CIPs, CIPs@Fe₂O₃ and CIPs@FeO@C composites, as shown in Fig. 6a, the RL values with different thickness enhance with the increase of frequency in the measurement range, the maximum RL is only -1.97 dB at 3 GHz for the thickness of 2 mm, although this value will increase to -6.41 dB as the thickness added to 6 mm, indicating the electromagnetic absorption performance of raw CIPs is still very limited. This situation will be improved for the

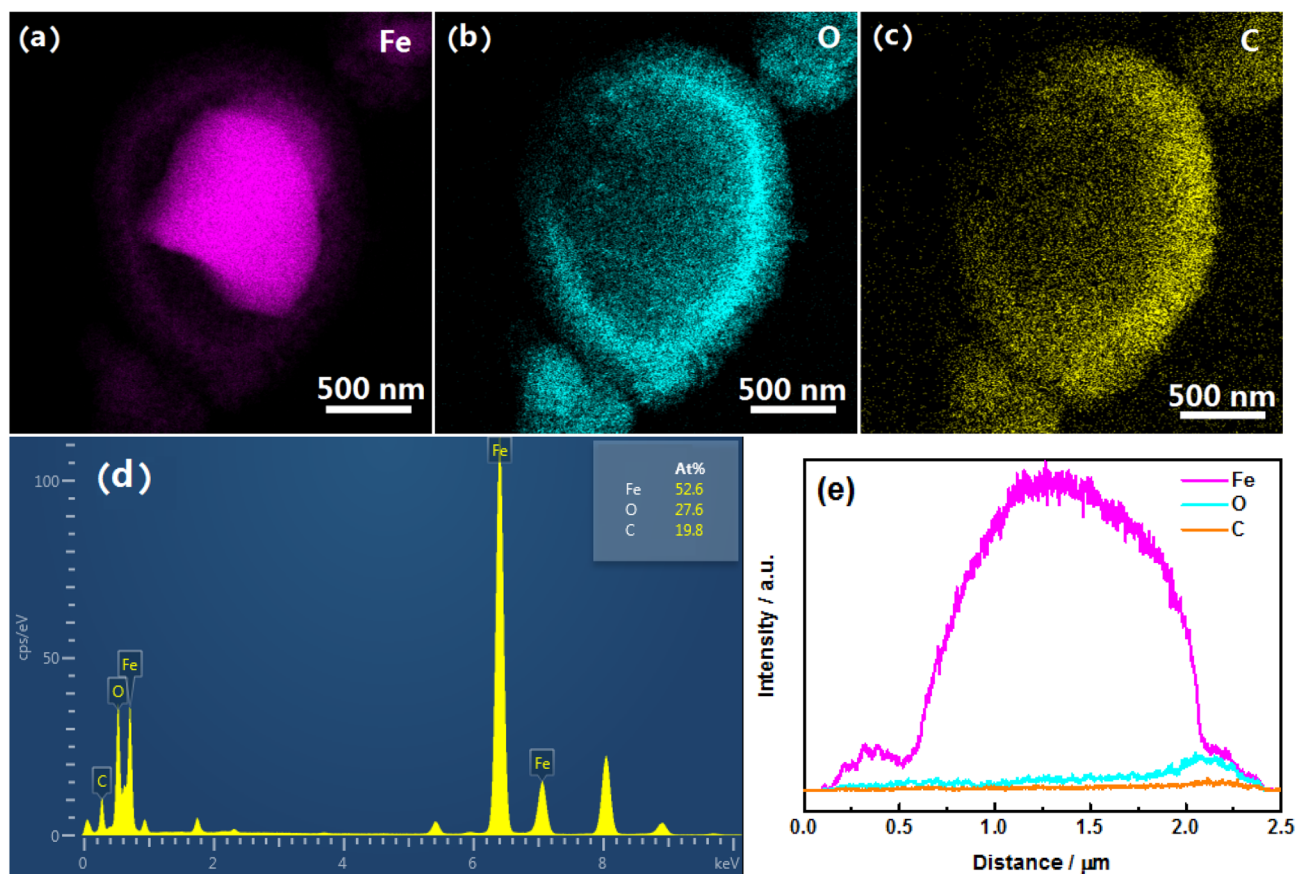


Fig. 5 Elements distribution of Fe (a), O (b), C (c), EDS spectrum (d) and linear distribution of elements (e) in CIPs@FeO@C composite

cladding of Fe_2O_3 NPs around CIPs to form the core-shell structure, as shown in Fig. 6b, the maximum RL at 2 mm thickness enhances to -7.48 dB at 3 GHz, and the effective absorption frequency range below -10 dB begins to appear as the thickness is greater than 3 mm, usually over 90% energy of electromagnetic-wave will be consumed away when the reflection loss of absorber is lower than -10 dB [27]. Moreover, the peak of maximum RL can be seen as the thickness is 5 mm, which would be further increased with the thickness enlarged to 6 mm, the maximal RL is -21.88 dB at 2.59 GHz with an effective absorption bandwidth of $\text{RL} < -10$ dB between 1.99 and 3 GHz at this thickness. In addition, the effective absorption bandwidths of this binary composite under different thickness of 2–6 mm are 0 GHz, 0.17 GHz, 0.49 GHz, 0.77 GHz and 1.01 GHz, respectively. Figure 6c displays the RL values of CIPs@FeO@C composite with various thicknesses, it can be noted that the electromagnetic-wave absorbing property has been further strengthened, which is mainly embodied in the extension of effective absorption bandwidth enhanced to 0.25 GHz, 0.84 GHz, 1.20 GHz, 1.15 GHz and 1.04 GHz for 2–6 mm thickness. The maximum RL of peak further achieves -24.64 dB at 1.88 GHz with an effective

absorption bandwidth of 1.39–2.43 GHz at 6 mm thickness. Furthermore, because of the quarter-wavelength resonance effectiveness, the RL peaks would shift to the low-frequency region when the thickness of composite added [28, 29].

3.3 Microwave absorption mechanism analysis

To further explore the possible mechanism for enhanced electromagnetic absorbing performance of ternary core-shell-shell composite, the relative permeability ($\mu = \mu' - j\mu''$) and permittivity ($\epsilon = \epsilon' - j\epsilon''$) of raw CIPs, CIPs@ Fe_2O_3 and CIPs@FeO@C composite are displayed in Fig. 7. As shown in Fig. 7a, the ϵ' of raw CIPs is about 2.3–2.5 with little change in the whole frequency range, while the real part of permittivity in binary composite increases obviously due to the dielectric property of ferrite and core-shell structure, it decreases slightly from 4.95 to 3.84 with the increase of frequency. This enhancement of ϵ' will be further reinforced in carbon-encapsulated CIPs@FeO ternary composite, especially in the low-frequency range, the ϵ' decreases from 7.06 to 4.04 with the increase of frequency. Figure 7b presents that the imaginary part of permittivity in raw CIPs is also very low in the measurement range,

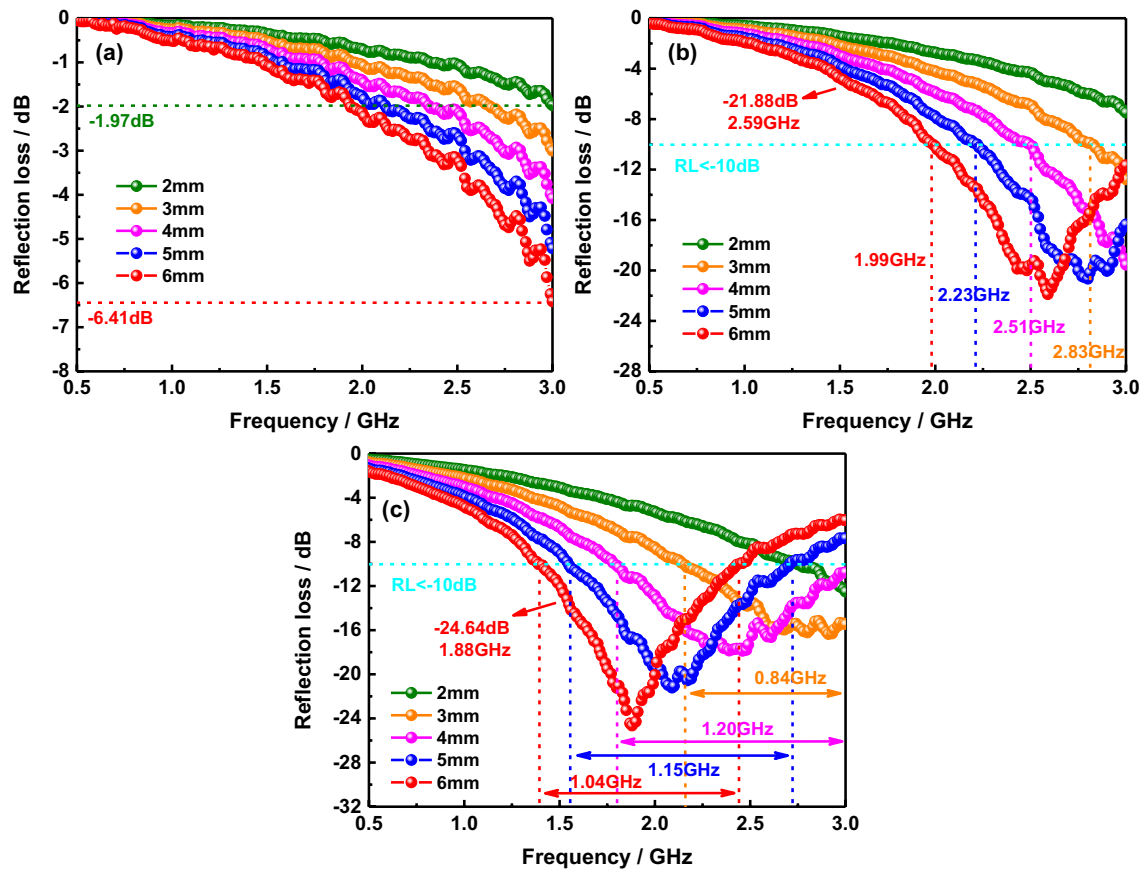


Fig. 6 Microwave reflection loss curves of raw CIPs (a), CIPs@Fe₂O₃ (b) and CIPs@FeO@C (c)

the ϵ'' in relatively high frequency domain would increase in the binary composite and it will be further enhanced among the whole frequency range in ternary composite, indicating that this carbon-encapsulated CIPs@FeO composite may possess a better dielectric loss capacity, for the imaginary part in electromagnetic parameters often reflects its abrasive ability of microwave energy [30]. Moreover, as shown in Fig. 7c and d, the real and imaginary part of permeability in three samples are all increasing with the enhancement of frequency. However, it indicates that the μ' and μ'' in raw CIPs are comparatively low, and these magnetic parameters will be strengthened as the CIPs encased with Fe₂O₃ NPs due to the excellent magnetic properties of iron sesquioxide [31]. When the Fe₂O₃ component is restored to FeO in carbon-encapsulated CIPs@FeO composite, it suggests that the μ' and μ'' of ternary composite would be further heightened. This is owing to that the interface between ferromagnetic (FM) CIPs and antiferromagnetic (AFM) FeO plays a significant role in determining the magnetic properties of composite, there exists an intensely exchange interaction between CIPs and FeO layer, which would lead to the exchange bias phenomenon and promote magnetic parameters [32, 33]. Thus, the magnetic property of as-prepared core-shell-shell

composite is the best among all the samples, which may be an intuitive reason for its better performance in electromagnetic absorption.

Figure 8 presents the tangents of magnetic and dielectric loss in raw CIPs, CIPs@Fe₂O₃ and CIPs@FeO@C composites. In Fig. 8a, it exhibits that the tangent of dielectric loss in raw CIPs increases firstly and then decreases as the frequency increased, there is a peak value of 0.11 at 2.49 GHz, suggesting a weak dielectric loss ability of microwave in raw CIPs. However, this tangent of dielectric loss will be enhanced in the relatively high frequency domain in binary core-shell composite, and it will be further heightened during the whole frequency range in ternary composite, which increases from 0.07 to 0.25 when the frequency increased, implying a better dielectric loss performance of CIPs@FeO@C composite compared with the other two MAMs. As shown in Fig. 8b, homoplastically the tangent of magnetic loss in raw CIPs is relatively low, and this tangent will be gradually enhanced in the measurement frequency range corresponding to CIPs@Fe₂O₃ and CIPs@FeO@C composites, indicating the preferable magnetic loss property of ternary composite on the whole range. It is worth noting that the small peaks in

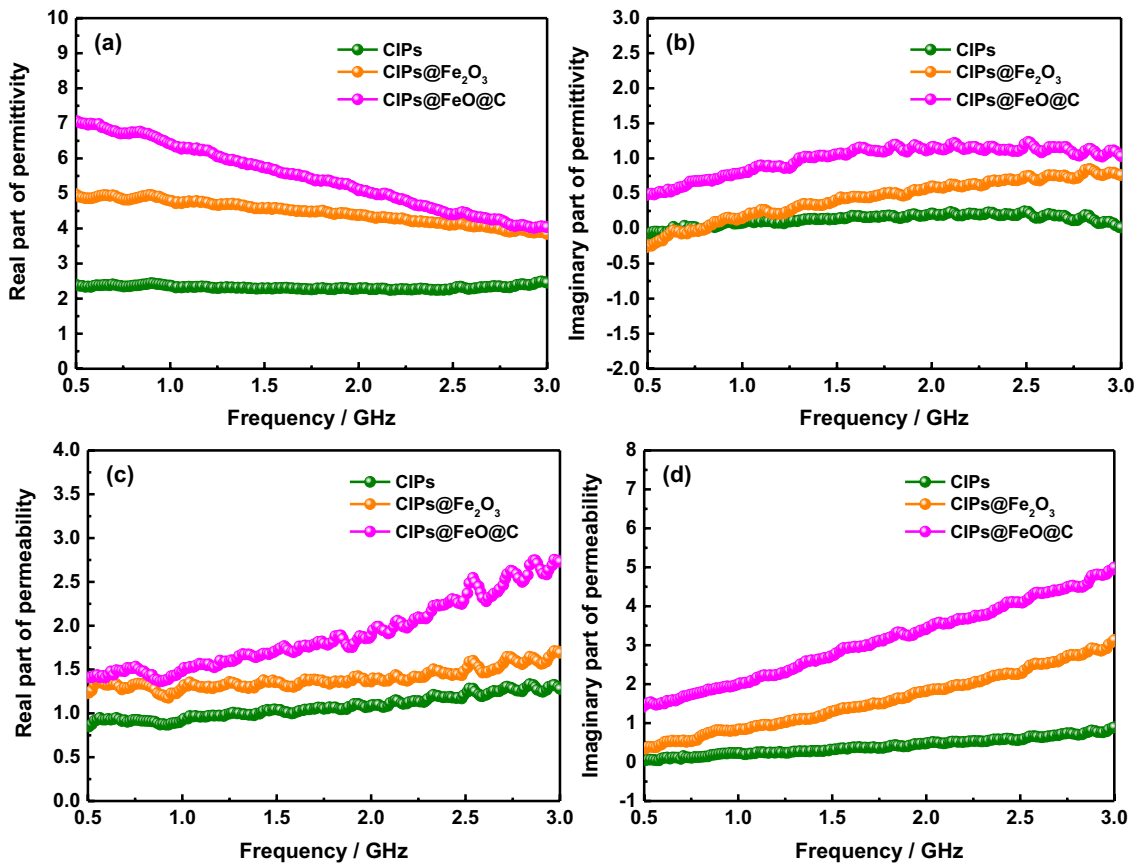


Fig. 7 Relative permittivity and permeability of raw CIPs, CIPs@Fe₂O₃ and CIPs@FeO@C composites

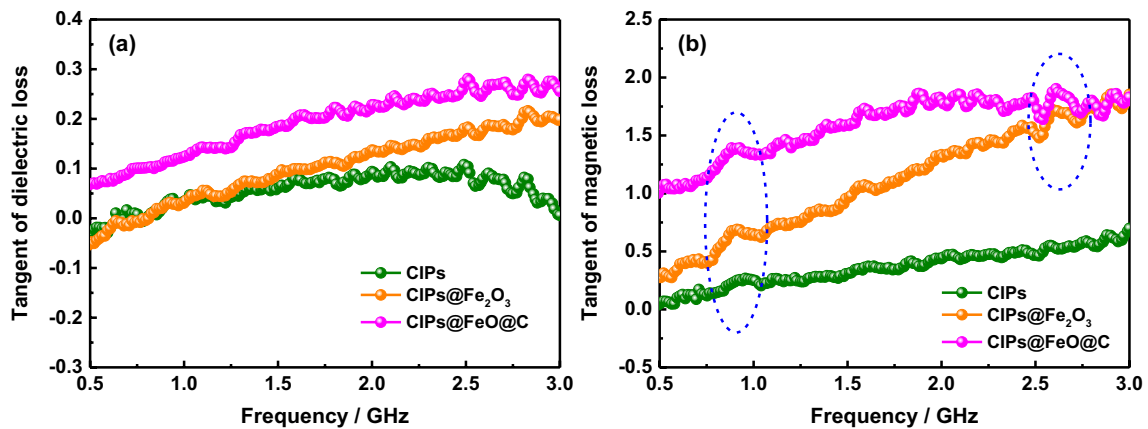


Fig. 8 Tangents of dielectric loss and magnetic loss in raw CIPs, CIPs@Fe₂O₃ and CIPs@FeO@C composites

curves of magnetic loss tangent are attributed to the natural ferromagnetic resonance phenomenon of composites.

Furthermore, the eddy current loss is often one important cause for magnetic loss in GHz range apart from natural resonance, hysteresis loss and domain wall resonance

[34, 35], which can be characterized by the following parameter C_0 [36]:

$$C_0 = \mu''(\mu')^{-2}f^{-1} \approx 2\pi\mu_0\sigma d^2/3 \quad (3)$$

It indicates that if the eddy current loss has a role in magnetic loss of microwave, the characterization parameter C_0 will remain the constant. Figure 9a suggests that C_0 parameters of raw CIPs and CIPs@Fe₂O₃ composite almost unchanged with the increase of frequency; however, this parameter of CIPs@FeO@C composite decreases with exponential relationship as frequency increased, confirming the eddy current loss may be an important factor to promote magnetic loss of ternary composite resulting in the enhanced microwave absorbing performance. Besides, the attenuation

constant also affects the electromagnetic absorption properties of as-prepared composites and can be deduced by the following equation [37, 38]:

$$\alpha = \frac{\sqrt{2\pi}f}{c} \times \sqrt{(\mu''\epsilon'' - \mu'\epsilon') + \sqrt{(\mu''\epsilon'' - \mu'\epsilon')^2 + (\mu'\epsilon'' + \mu''\epsilon')^2}} \quad (4)$$

As shown in Fig. 9b, the attenuation constants of raw CIPs and CIPs@Fe₂O₃ composite increase from 0.18 to

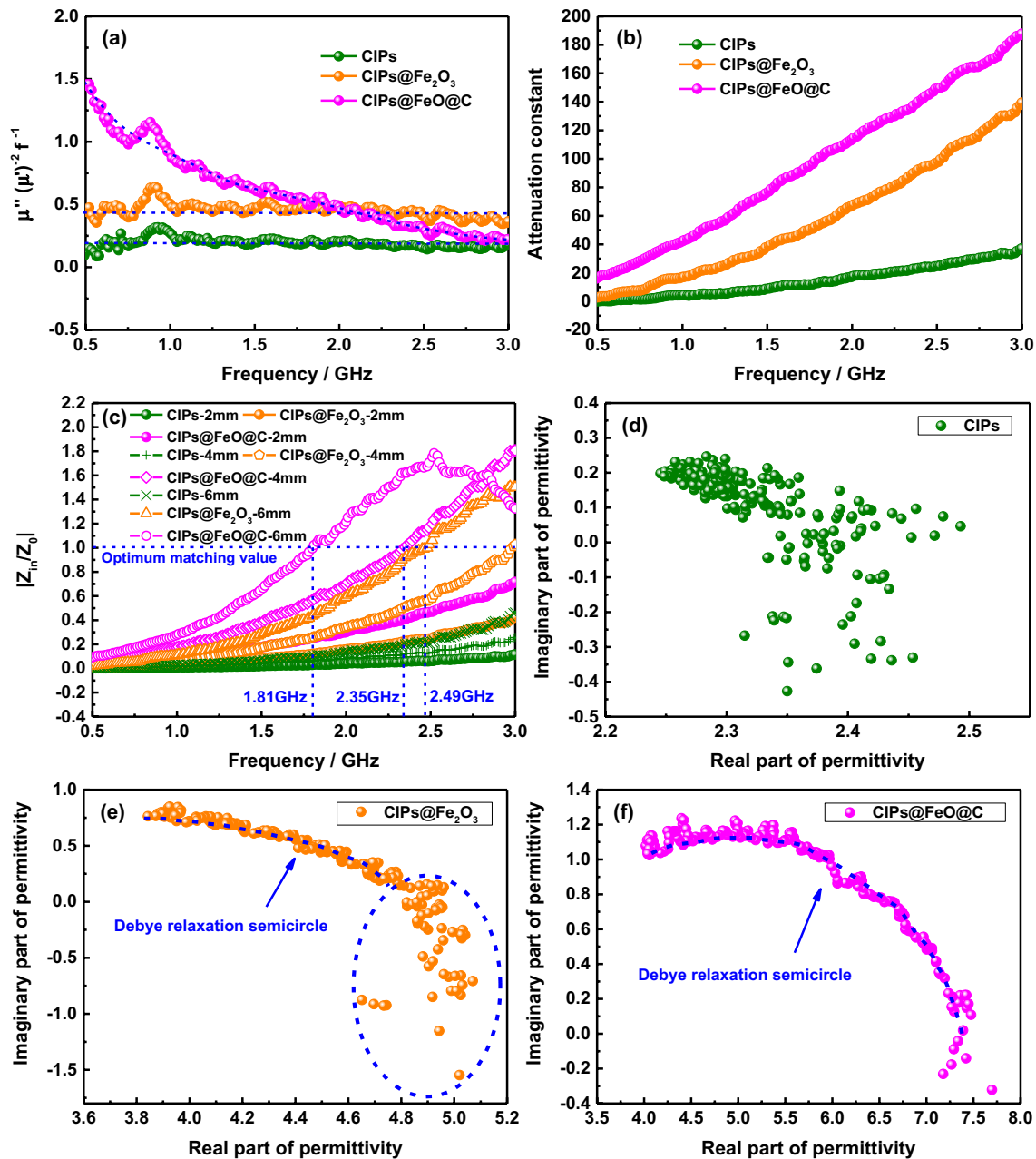


Fig. 9 Eddy current loss curves (a), attenuation constants (b), frequency dependent $|Z_{in}/Z_0|$ values with different thicknesses (c) and plots of $\epsilon'-\epsilon''$ (d) to (f) in raw CIPs, CIPs@Fe₂O₃ and CIPs@FeO@C composites

Table 1 Comparison of electromagnetic absorption properties between CIPs@FeO@C and related CIPs composites reported in other literatures

Materials	Thickness (mm)	Minimum RL (dB)	Position (GHz)	RL < -10 dB (GHz)	Refs
C@CIPs	0.6	-5.48	9.3	-	[44]
rGO/MCI/PVP	2.8	-41.76	10	5.48–18	[45]
R-GO/F-CIP/PANI	2	-38.8	11.8	-	[46]
Cl/rGO	2.5	-103.8	7.8	5.48–11.28	[47]
Cl/rGO/PVP	1.5	-31.81	16.88	8.12–18	[47]
Cl/rGO/PVP	2.5	-29.79	9.68	5.08–18	[47]
Cl/rGO/PVP	4.8	-35	3.04	2–18	[47]
Oriented FCI/EP-A	1.5	-13	3.5	-	[48]
Oriented FCI/EP-B	1.4	-	-	5.5–18	[48]
FCI	1.5	-15.7	6	4.5–8.5	[49]
RGO-SCI	3	-52.46	9.46	7.79–11.98	[50]
CIPs@FeO@C	3	-16.35	2.91	2.16–3	This work
CIPs@FeO@C	4	-17.39	2.29	1.8–3	This work
CIPs@FeO@C	5	-21.21	2.09	1.55–2.7	This work
CIPs@FeO@C	6	-24.64	1.88	1.39–2.43	This work

37.24 and 2.96 to 139.44, respectively, which indicates that the CIPs@Fe₂O₃ core-shell hybrid possesses the better microwave attenuation capacity, while this attenuation parameter would be further enlarged to 17.04–187.79 in CIPs@FeO@C composite, explaining the reasonable reason for its preminent electromagnetic absorption within the low-frequency band.

Figure 9c shows the impedance matching characteristic of $|Z_{in}/Z_0|$ in raw CIPs, CIPs@Fe₂O₃ and CIPs@FeO@C composites at different thickness of 2 mm, 4 mm and 6 mm. It can be noted that the $|Z_{in}/Z_0|$ values of raw CIPs are much less than one, leading to a poor electromagnetic-wave absorption properties of the sample. The $|Z_{in}/Z_0|$ values will be successively increased in CIPs@Fe₂O₃ and CIPs@FeO@C composites, respectively, standing for the improved impedance matching properties. The optimum matching values of CIPs@Fe₂O₃ and CIPs@FeO@C at thickness of 4 mm and 6 mm appear at the frequency of 2.99 GHz, 2.49 GHz, 2.35 GHz and 1.81 GHz, which are almost in line with the position of the maximum RL peaks in these composites at corresponding thickness, clarifying a fact that the impedance matching property in composites plays a significant role in determining their microwave absorbing performance. This is due to that more electromagnetic-wave can transmit into MAMs to be further worn out by multiple microwave loss mechanism with excellent impedance matching status [39–41]. Hence, the improved microwave absorbing performance of ternary composite is ascribed to this cause in some extent. Moreover, the Debye relaxation may be another significant reason to motivate the dielectric loss in samples, the relation between ϵ' and ϵ'' can be induced according to the theory of Debye's [42, 43]:

$$\left(\epsilon' - \frac{\epsilon_s + \epsilon_\infty}{2}\right)^2 + (\epsilon'')^2 = \left(\frac{\epsilon_s - \epsilon_\infty}{2}\right)^2 \quad (5)$$

The Eq. (5) denotes the Cole–Cole semicircle of real and imaginary part of permittivity in Debye relaxation process. As shown in Fig. 9d, no obvious Cole–Cole semicircle can be observed declaring that negligible Debye relaxation occurs in the raw CIPs for poor electromagnetic absorption. However, the partial Cole–Cole semicircle of CIPs@Fe₂O₃ composite in Fig. 9e indicates a weak Debye relaxation for dielectric absorption of incident microwave in this sample. In Fig. 9f, it is interesting to note that there exists a clear Cole–Cole semicircle with slight fluctuation in CIPs@FeO@C composite, illustrating the Debye relaxation makes a contribution to the dielectric loss for enhanced microwave absorption in this ternary composite.

Table 1 summarizes the electromagnetic-wave absorption properties of related CIPs-based composites in other literatures and this work [44–50]. It can be seen from table that the effective absorbing range of other CIPs-based composites are mainly focus in the relatively high frequency band. Although the thickness of electromagnetic absorber prepared here is a little thick, the microwave absorption range of as-prepared CIPs@FeO@C composite is located in the low-frequency band with advisable intensity and the preparation method is simple and economical. Hence, it can be used as an efficient low-frequency MAMs in deed.

4 Conclusion

In summary, the CIPs@FeO@C composite has been synthesized successfully via a novel co-calcine, high temperature thermal diffusion and reduction method with activated carbon as carbon source and reducing agent. The as-prepared composite possesses a multilayer core-shell-shell structure consisting of various components with different electromagnetic absorption mechanisms, hence the synergistic effect of magnetic and dielectric loss contributes to the low-frequency electromagnetic-wave absorbing performance of this ternary composite. The maximum RL value achieves -24.64 dB at 1.88 GHz for 6 mm thickness and the broadest effective absorbing bandwidth (RL < -10 dB) reaches 1.2 GHz in low-frequency band for 4 mm thickness. Compared to raw CIPs, the relatively higher imaginary part of permittivity and permeability, good impedance matching property, outstanding attenuation characteristic, efficient eddy current loss, Debye relaxation and interfacial polarization endow the composite advisable low-frequency microwave absorption ability.

Acknowledgments This work is supported by the Grants from National Natural Science Foundation of China (Nos. 61701050 and 51704242), the Project of Sichuan Provincial Department of Education (No. 2018Z073), and the Natural Science Foundation of Shaanxi Province in China (No. 2018JM5094).

References

- Z. Jia, D. Lan, K. Lin, M. Qin, K. Kou, G. Wu, H. Wu, Progress in low-frequency microwave absorbing materials. *J. Mater. Sci. Mater. Electron.* **29**, 17122–17136 (2018)
- X. Zhang, J. Xiang, Z. Wu, L. Gong, X. Chen, G. Guan, Y. Wang, K. Zhang, Enhanced absorbing properties and structural design of microwave absorbers based on $\text{Ni}_{0.8}\text{Co}_{0.2}\text{Fe}_2\text{O}_4$ nanofibers and Ni-C hybrid nanofibers. *J. Alloys Compd.* **764**, 691–700 (2018)
- D. Lan, M. Qin, R. Yang, S. Chen, H. Wu, Y. Fan, Q. Fu, F. Zhang, Facile synthesis of hierarchical chrysanthemum-like copper cobaltate-copper oxide composites for enhanced microwave absorption performance. *J. Colloid Inter. Sci.* **533**, 481–491 (2019)
- Z. Jia, K. Lin, G. Wu, H. Xing, H. Wu, Recent progresses of high-temperature microwave-absorbing materials. *NANO* **13**, 1830005 (2018)
- H. Wu, G. Wu, Y. Ren, L. Yang, L. Wang, X. Li, $\text{Co}^{2+}/\text{Co}^{3+}$ ratio dependence of electromagnetic wave absorption in hierarchical $\text{NiCo}_2\text{O}_4\text{-CoNiO}_2$ hybrids. *J. Mater. Chem. C* **3**, 7677–7690 (2015)
- J. Xiang, Z. Hou, X. Zhang, L. Gong, Z. Wu, J. Mi, Facile synthesis and enhanced microwave absorption properties of multiferroic $\text{Ni}_{0.4}\text{Co}_{0.2}\text{Zn}_{0.4}\text{Fe}_2\text{O}_4/\text{BaTiO}_3$ composite fibers. *J. Alloys Compd.* **737**, 412–420 (2018)
- R. Shu, G. Zhang, J. Zhang, X. Wang, M. Wang, Y. Gan, J. Shi, J. He, Synthesis and high-performance microwave absorption of reduced graphene oxide/zinc ferrite hybrid nanocomposite. *Mater. Lett.* **215**, 229–232 (2018)
- R. Shu, W. Li, Y. Wu, J. Zhang, G. Zhang, Nitrogen-doped Co-C/MWCNTs nanocomposites derived from bimetallic metal-organic frameworks for electromagnetic wave absorption in the X-band. *Chem. Eng. J.* **362**, 513–524 (2019)
- X. Zhang, Y. Zhang, B. Tian, Y. Jia, M. Fu, Y. Liu, K. Song, A.A. Volinsky, X. Yang, H. Sun, Graphene oxide effects on the properties of $\text{Al}_2\text{O}_3\text{-Cu}/35\text{W5Cr}$ composite. *J. Mater. Sci. Technol.* **37**, 185–199 (2020)
- M.M. Ismail, S.N. Rafeeq, J.M.A. Sulaiman, A. Mandal, Electromagnetic interference shielding and microwave absorption properties of cobalt ferrite CoFe_2O_4 /polyaniline composite. *Appl. Phys. A* **124**, 380 (2018)
- S. Yun, A. Kirakosyan, S. Surabhi, J.R. Jeong, J. Choi, Controlled morphology of MWCNTs driven by polymer-grafted nanoparticles for enhanced microwave absorption. *J. Mater. Chem. C* **5**, 8436–8443 (2017)
- O. Khani, M.Z. Shoushtari, K. Ackland, P. Stamenov, The structural, magnetic and microwave properties of spherical and flake shaped carbonyl iron particles as thin multilayer microwave absorbers. *J. Magn. Magn. Mater.* **428**, 28–35 (2017)
- Y. Xu, L. Yuan, Z. Liang, X. Wang, X. Li, A wide frequency absorbing material added CIPs using the fuse deposition modeling. *J. Alloys Compd.* **704**, 593–598 (2017)
- W. Hong, S. Dong, P. Hua, X. Luo, S. Du, In situ growth of one-dimensional nanowires on porous PDC-SiC/Si₃N₄ ceramics with excellent microwave absorption properties. *Ceram. Inter.* **43**, 14301–14308 (2017)
- L. Gao, W. Zhou, F. Luo, D. Zhu, J. Wang, Dielectric and microwave absorption properties of KNN/ Al_2O_3 composite ceramics. *Ceram. Inter.* **43**, 12731–12735 (2017)
- R.B. Yang, W.F. Liang, Microwave properties of high-aspect-ratio carbonyl iron/epoxy absorbers. *J. Appl. Phys.* **109**, 07A311 (2011)
- Y. Zuo, Z. Yao, H. Lin, J. Zhou, J. Lu, J. Ding, Digital light processing 3D printing of graphene/carbonyl iron/polymethyl methacrylate nanocomposites for efficient microwave absorption. *Compos. Part B* **179**, 107533 (2019)
- J. Dong, W. Zhou, C. Wang, L. Lu, F. Luo, D. Zhu, Anisotropic particle geometry effect on magnetism and microwave absorption of carbonyl iron/polyimide composites. *J. Magn. Magn. Mater.* **491**, 165643 (2019)
- X. Chai, D. Zhu, D. Min, W. Zhou, Y. Qing, F. Luo, Flexible thin microwave absorbing patch: flake carbonyl iron and chopped carbon fibers oriented in resin matrix. *J. Mater. Sci. Mater. Electron.* **31**, 1442–1450 (2020)
- H. Nan, Y. Qing, H. Gao, H. Jia, F. Luo, W. Zhou, Synchronously oriented Fe microfiber & flake carbonyl iron/epoxy composites with improved microwave absorption and lightweight feature. *Compos. Sci. Technol.* **184**, 107882 (2019)
- W. Dai, F. Chen, H. Luo, Y. Xiong, X. Wang, Y. Cheng, R. Gong, Synthesis of yolk-shell structured carbonyl iron@void@nitrogen doped carbon for enhanced microwave absorption performance. *J. Alloys Compd.* **812**, 152083 (2020)
- A.M. Nicolson, G.F. Ross, Measurement of the intrinsic properties of materials by time-domain techniques. *IEEE Trans. Instrum. Meas.* **19**, 377–382 (1970)
- W.B. Weir, Automatic measurement of complex dielectric constant and permeability at microwave frequencies. *Proc. IEEE* **62**, 33–36 (1974)
- M. Qin, D. Lan, J. Liu, H. Liang, L. Zhang, H. Xing, T. Xu, H. Wu, Synthesis of single-component metal oxides with controllable multi-shelled structure and their morphology-related applications. *Chem. Rec.* **20**, 102–119 (2020)
- D. Lan, M. Qin, R. Yang, H. Wu, Z. Jia, K. Kou, G. Wu, Y. Fan, Q. Fu, F. Zhang, Synthesis, characterization and microwave transparent properties of Mn_3O_4 microspheres. *J. Mater. Sci. Mater. Electron.* **30**, 8771–8776 (2019)

26. P. Liu, V.M.H. Ng, Z. Yao, J. Zhou, Y. Lei, Z. Yang, H. Lv, L.B. Kong, Facile synthesis and hierarchical assembly of flowerlike NiO structures with enhanced dielectric and microwave absorption properties. *ACS Appl. Mater. Inter.* **9**, 16404–16416 (2017)
27. Y. Du, W. Liu, R. Qiang, Y. Wang, X. Han, J. Ma, P. Xu, Shell thickness-dependent microwave absorption of core-shell Fe₃O₄@C composites. *ACS Appl. Mater. Inter.* **6**, 12997–13006 (2014)
28. M. Qiao, X. Lei, Y. Ma, L. Tian, X. He, K. Su, Q. Zhang, Application of yolk-shell Fe₃O₄@N-doped carbon nanochains as highly effective microwave-absorption material. *Nano Res.* **11**, 1500–1519 (2018)
29. R. Li, T. Wang, G.G. Tan, W.L. Zuo, J.Q. Wei, L. Qiao, F.S. Li, Microwave absorption properties of oriented Pr₂Fe₁₇N₃₋₅ particles/paraffin composite with planar anisotropy. *J. Alloys Compd.* **586**, 239–243 (2014)
30. X.F. Liu, X.R. Cui, Y.X. Chen, X.J. Zhang, R.H. Yu, G.S. Wang, H. Ma, Modulation of electromagnetic wave absorption by carbon shell thickness in carbon encapsulated magnetite nanospindles-poly (vinylidene fluoride) composites. *Carbon* **95**, 870–878 (2015)
31. H. Wu, G. Wu, L. Wang, Peculiar porous α -Fe₂O₃, γ -Fe₂O₃ and Fe₃O₄ nanospheres: facile synthesis and electromagnetic properties. *Powder Technol.* **269**, 443–451 (2015)
32. I.S. Lyubutin, C.R. Lin, Y.T. Tseng, A. Spivakov, A.O. Baskakov, S.S. Starchikov, K.O. Funtov, C.J. Jhang, Y.J. Tsai, H.S. Hsu, Structural and magnetic evolution of Fe_xO_y@carbon core-shell nanoparticles synthesized by a one-step thermal pyrolysis. *Mater. Charact.* **150**, 213–219 (2019)
33. A. Kozioł-Rachwał, W. Janus, M. Szpytma, P. Dróżdź, M. Ślęzak, K. Matlak, M. Gajewska, T. Ślęzak, J. Korecki, Interface engineering towards enhanced exchange interaction between Fe and FeO in Fe/MgO/FeO epitaxial heterostructures. *Appl. Phys. Lett.* **115**, 141603 (2019)
34. J. Fang, T. Liu, Z. Chen, Y. Wang, W. Wei, X. Yue, Z. Jiang, A wormhole-like porous carbon/magnetic particles composite as an efficient broadband electromagnetic wave absorber. *Nanoscale* **8**, 8899–8909 (2016)
35. Q. Long, Z. Xu, H. Xiao, K. Xie, A facile synthesis of a cobalt nanoparticle-graphene nanocomposite with high-performance and triple-band electromagnetic wave absorption properties. *RSC Adv.* **8**, 1210–1217 (2018)
36. Y. Lei, Z. Yao, H. Lin, J. Zhou, A.A. Haidry, P. Liu, The effect of polymerization temperature and reaction time on microwave absorption properties of Co-doped ZnNi ferrite/polyaniline composites. *RSC Adv.* **8**, 29344–29355 (2018)
37. B. Zhao, X.Q. Guo, W.Y. Zhao, J.H. Deng, B.B. Fan, G. Shao, Z.Y. Bai, R. Zhang, Facile synthesis of yolk-shell Ni@void@SnO₂(Ni₃Sn₂) ternary composites via galvanic replacement/Kirkendall effect and their enhanced microwave absorption properties. *Nano Res.* **10**(1), 331–343 (2017)
38. H. Wang, D. Zhu, X. Wang, F. Luo, Influence of silicon carbide fiber (SiCf) type on the electromagnetic microwave absorbing properties of SiCf/epoxy composites. *Compos. Part A* **93**, 10–17 (2017)
39. T. Liu, N. Liu, S. Zhai, S. Gao, Z. Xiao, Q. An, D. Yang, Tailor-made core/shell/shell-like Fe₃O₄@SiO₂@PPy composites with prominent microwave absorption performance. *J. Alloys Compd.* **779**, 831–843 (2019)
40. H. Lv, H. Zhang, J. Zhao, G. Ji, Y. Du, Achieving excellent bandwidth absorption by a mirror growth process of magnetic porous polyhedron structures. *Nano Res.* **6**, 1813–1822 (2016)
41. H. Lv, G. Ji, W. Liu, H. Zhang, Y. Du, Achieving hierarchical hollow carbon@Fe@Fe₃O₄ nanospheres with superior microwave absorption properties and lightweight features. *J. Mater. Chem. C* **3**, 10232–10241 (2015)
42. Z.J. Guan, J.T. Jiang, N. Chen, Y.X. Gong, L. Zhen, Carbon-coated CoFe-CoFe₂O₄ composite particles with high and dual-band electromagnetic wave absorbing properties. *Nanotechnology* **29**, 305604 (2018)
43. M. Zong, Y. Huang, Y. Zhao, X. Sun, C. Qu, D. Luo, J. Zheng, Facile preparation, high microwave absorption and microwave absorbing mechanism of RGO-Fe₃O₄ composites. *RSC Adv.* **3**, 23638–23648 (2013)
44. T. Liu, L. Zhou, D. Zheng, Y. Xu, Absorption property of C@CIPs composites by the mechanical milling process. *Appl. Phys. A* **123**, 565 (2017)
45. X. Weng, X. Lv, B. Li, Y. Zhang, H. Lou, P. Zhu, G. Gu, One-pot preparation of reduced graphene oxide/carbonyl iron/polyvinyl pyrrolidone ternary nanocomposite and its synergistic microwave absorbing properties. *Mater. Lett.* **188**, 280–283 (2017)
46. Y. Xu, J. Luo, W. Yao, J. Xu, T. Li, Preparation of reduced graphene oxide/flake carbonyl iron powders/polyaniline composites and their enhanced microwave absorption properties. *J. Alloys Compd.* **636**, 310–316 (2015)
47. X. Weng, B. Li, Y. Zhang, X. Lv, G. Gu, Synthesis of flake shaped carbonyl iron/reduced graphene oxide/polyvinyl pyrrolidone ternary nanocomposites and their microwave absorbing properties. *J. Alloys Compd.* **695**, 508–519 (2017)
48. D. Min, W. Zhou, Y. Qing, F. Luo, D. Zhu, Greatly enhanced microwave absorption properties of highly oriented flake carbonyl iron/epoxy resin composites under applied magnetic field. *J. Mater. Sci.* **52**, 2373–2383 (2017)
49. P. Ji, G. Xie, N. Xie, J. Li, J. Chen, J. Chen, Microwave absorbing properties of flaky carbonyl iron powder prepared by rod milling method. *J. Electron. Mater.* **48**, 2495–2500 (2019)
50. Z.T. Zhu, X. Sun, H.R. Xue, H. Guo, X.L. Fan, X.C. Pan, J.P. He, Graphene-carbonyl iron cross-linked composites with excellent electromagnetic wave absorption properties. *J. Mater. Chem. C* **2**, 6582–6591 (2014)

Publisher's Note Springer Nature remains neutral with regard to jurisdictional claims in published maps and institutional affiliations.